Organic Electronics 13 (2012) 184–194

Contents lists available at SciVerse ScienceDirect

Organic Electronics

journal homepage: www.elsevier.com/locate/orgel

Optical and thermal properties of large-area OLED lightings with metallic grids

Jongwoon Park [a,*], Jongho Lee [a], Yong-Young Noh [b]

[a] OLED Lighting Team, National Center for Nanoprocess and Equipment, Korea Institute of Industrial Technology, Gwangju 500-480, Republic of Korea
[b] Department of Chemical Engineering, Hanbat National University, Daejeon 305-71, Republic of Korea

ARTICLE INFO

Article history:
Received 28 July 2011
Received in revised form 10 October 2011
Accepted 23 October 2011
Available online 23 November 2011

Keywords:
Organic light-emitting diodes (OLEDs)
Transparent OLEDs
Auxiliary electrode
Metallic grids
Heat distribution

ABSTRACT

We investigate the effects of auxiliary metal electrodes on the optical and thermal properties of large-area (30×120 mm^2) opaque and transparent white OLED lighting panels. Enlarging their emission area inevitably entails a non-uniform current distribution due to the limiting conductivity of transparent electrodes, causing local heat generation. To tackle it, we have used grid patterned Cr, Mo/Al/Mo, or Cu metal lines (0.15 mm in width) as auxiliary metal electrodes on an ITO anode. Among those, Cu metal grids exhibit the highest luminous efficacy with the least heat generation, and the most uniform light distribution by virtue of its lowest sheet resistance, followed by Mo/Al/Mo and then Cr metal grids. It is also found that local heat generation appears more seriously in large-area transparent OLED panels. With attempt to suppress it, we have also deposited Al metal lines (2 mm in width) on a semitransparent Al/Ag cathode by thermal evaporation, which brings in a highly uniform heat distribution. Furthermore, we study the effect of the shape of the light-emitting area on the luminance and heat distributions. A round-shaped OLED panel with a hexagonal metal grid exhibits highly homogeneous luminance and surface temperature distributions.

1. Introduction

Continuous technological progress in the organic light-emitting diode (OLED) industry enables us to overcome major technology setbacks such as a relatively low power efficiency and short lifetime [1–3]. Thus, flat-panel OLED displays have already been commercialized and available in the market. However, there still exist many technical issues in the development of flat-panel OLED lightings. One of the most critical issues is to enlarge the size of surface-emitting OLED lighting panels to meet some required luminous flux [4,5]. This brings in several tricky problems, for example, a short circuit, non-uniform light emission, hot spot, power loss, and local heat generation [6–9]. Of those, non-uniform light emission, power loss, and local heat generation are directly related to the indium-tin-oxide (ITO) based transparent electrode used in OLED devices. Due to the limiting conductivity of the transparent electrode, current injected from the panel edges reaches hardly its central region, causing inhomogeneous light emission and heat distributions. This, in turn, gives rise to a power loss and consequently a reduction of the luminous efficacy [10]. Similar but worse phenomena may appear in large-area transparent OLED (TOLED) lighting panels due also to the low conductivity of a transparent cathode. As a transparent cathode, various structures have been studied such as Mg:Ag, Al/Ag, ITO/Ag/ITO, ITO/Ag/tungsten oxide (WO_3), WO_3/Ag/WO_3, etc. [11,12]. However, those electrodes still have a high sheet resistance ($\sim$6 Ω/□) since the transparency of panels can be obtained at a sacrifice of the sheet resistance. When both electrodes (anode and cathode) show relatively high resistance,

* Corresponding author.
E-mail address: pjwup75@kitech.re.kr (J. Park).

1566-1199/$ - see front matter © 2011 Elsevier B.V. All rights reserved.
doi:10.1016/j.orgel.2011.10.024

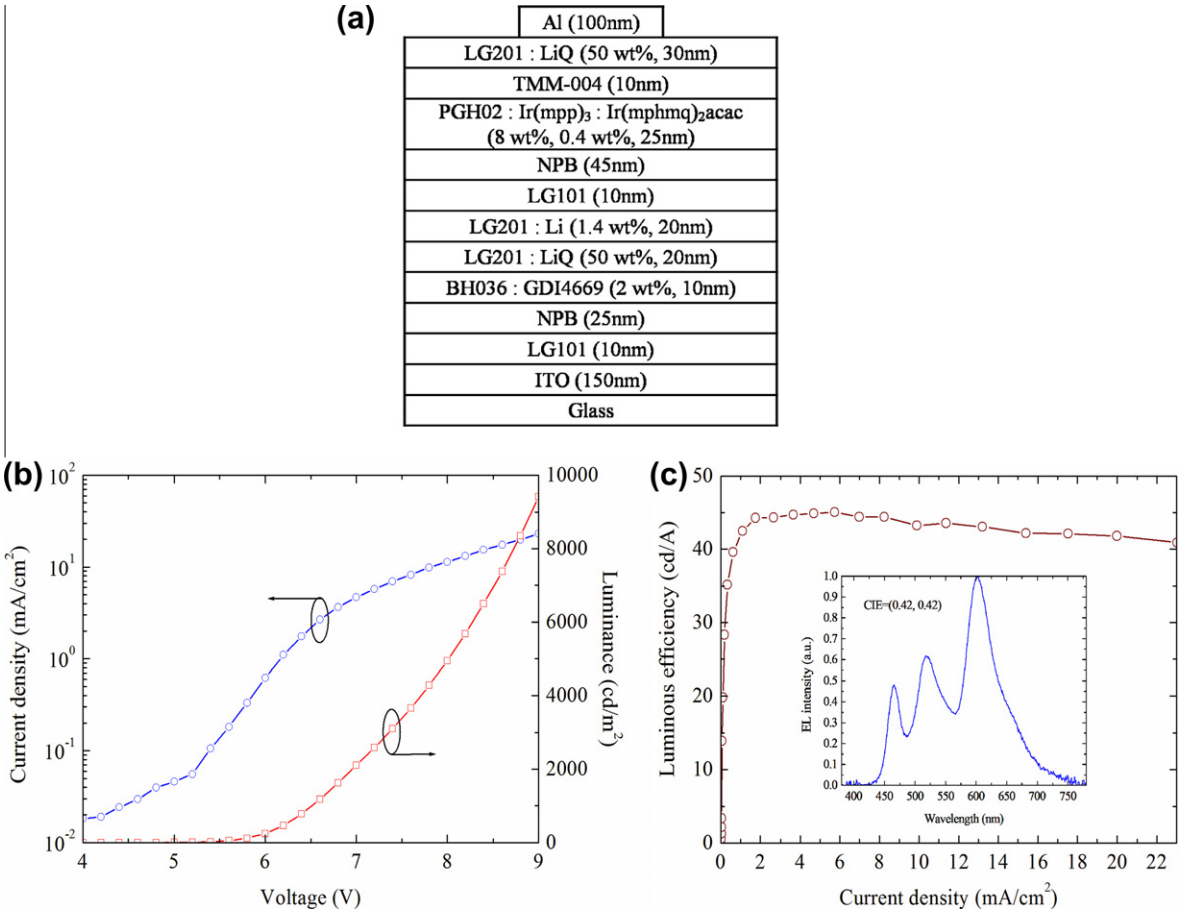

Fig. 1. (a) Layer structure, (b) current density and luminance versus bias voltage, and (c) luminous efficiency of the 2 mm × 2 mm hybrid tandem white OLED device. Inset in Fig. 1(c) shows the EL spectrum of the device.

non-uniform light emission, power loss, and local heat generation may become more pronounced.

A straightforward method for resolving those problems is to reduce the sheet resistance of transparent electrodes without decrease of transparency. The commonly used transparent electrode (i.e., ITO) for anode shows the sheet resistance of 9–12 Ω/□, which is still too high for large-area lighting panels. Another electrode structure employing a highly conductive metal (Ag) sandwiched between two conductive oxides has been introduced [13–15]. Although it provides lower sheet resistance (3–4 Ω/□), the multi-stacking of different materials makes the patterning process difficult. Another promising approach to realize highly conductive transparent electrodes is applying micro-sized metal grids on ITO as an auxiliary electrode [6,16]. In this configuration, current flows through the high-conductivity metal grids from the panel edges to the central region, yielding highly homogeneous light distribution over a large area. The effective sheet resistance of such a structure can be expressed as [16]

$$R_{eff} \approx \frac{2h}{\sigma w d} \tag{1}$$

where h is the apothem, w is the width, d is the thickness, and σ is the conductivity of metallic grids. In reality, there exists a tradeoff between the sheet resistance and the transmittivity of the grid on the selection of the ratio h/w since the transmittivity is determined by

$$T = 1 - \frac{w}{h}. \tag{2}$$

Namely, increasing metal coverage (w/h) lowers the effective sheet resistance, but at the same time reduces the transmittivity or rather the overall light-emitting area. Besides, the grid thickness (d) is also limited (typically 300–500 nm) because it should be covered with an insulating material on which very thin organic layers are then formed. Therefore, the conductivity (σ) of metallic grids is a key controllable parameter in reducing the effective sheet resistance and thus enhancing the device performance. To our best knowledge, there is no study to clarify the effect of auxiliary metal electrodes on the optical and thermal properties of large-area OLED and TOLED lighting panels.

In this paper, we investigate the effects of materials and grid patterns of auxiliary metal electrodes on the performance of large-area opaque and transparent white OLED lighting panels. We selected Cr, Mo/Al/Mo, and Cu as auxiliary metal electrodes on ITO anode due to their high conductivity, processability, stability, and a low material price.

Cr is mainly considered by virtue of its ease of patterning and good chemical resistance, even though it shows a relatively low conductivity. Mo/Al/Mo is one of promising candidates because its sheet resistance is dramatically reduced by using a thick Al metal [17]. In this structure, Mo is used to prevent an oxidization of Al and shows a good adhesion with Al. Moreover, the ingredients of etchant for Mo are very similar to those for Al. Cu metal is also favored because of its high conductivity, even though it is reactive to oxygen and thus easily oxidized. It is demonstrated that Cu metal grids exhibit the highest luminous efficacy with the least heat generation, and the most uniform light distribution due to its lowest sheet resistance, followed by Mo/Al/Mo and then Cr metal grids. We have also addressed that large-area TOLED panels require metallic grids not only on an anode but also on a semitransparent cathode to suppress local heat generation.

In addition to the conductivity of metallic grids, there exist more factors that affect emission uniformity, power loss, and local heat generation. Usually, the light-emitting area of panels is surrounded with patterned high-conductivity auxiliary metal (anode) to ensure uniform current injection. As such, its configuration is one of factors that affect those device performances. Another one is a contact resistance at the interface between the electrodes and a driving circuit. To reduce it, Ag pastes along with copper wires are commonly employed. Multi-pin contacts are also used to suppress the contact resistance as well as the current non-uniformity [6]. The other one lies in the shape of the light-emitting area. It is demonstrated that the hexagonal grid has the lowest average voltage loss, which is 6% lower than for the square grid [16]. In this context, a round-shaped panel is expected to show more uniform current and heat distributions. At the end, we have also studied the effect of the shape of light-emitting areas and metal grids on the luminance and heat distributions of large-area OLED lighting panels.

2. Experiment

For experiments, we fabricated a hybrid tandem white OLED device (Fig. 1(a)) that consists of a 150-nm-thick ITO pre-coated on a glass substrate, 10-nm-thick LG-101 for a hole injection layer (HIL), 25-nm-thick 4,4′-bis[*N*-(1-nathyl)-*N*-phenylamino]biphenyl (NPB) for a hole transport layer (HTL), 10-nm-thick BH036 for a fluorescent blue-emitting layer (Dow Advanced Display Materials Ltd.), 20-nm-thick LG-201 for an electron transport layer (ETL) doped with 50 wt.% lithium quinolate (LiQ), 30-nm-thick charge generation layer (CGL), 45-nm-thick NPB for a HTL, 25-nm-thick PGH-02 for a phosphorescent green- and red-emitting layer, 10-nm-thick TMM-004 for a hole/exciton blocking layer (HBL) (Merck), 30-nm-thick LG-201 for an ETL doped with 50 wt.% LiQ, and 100-nm-thick Al. In the blue-emitting layer, 2 wt.% GDI4669 is doped (Dow Advanced Display Materials Ltd.). The CGL layer is composed of 20-nm-thick LG201 doped with 1.4 wt.% Li and 10-nm-thick LG101. In the green- and red-emitting layer, 8 wt.% $Ir(mpp)_3$ and 0.4 wt.% $Ir(mphmq)_2acac$ [18] are co-doped. Presented in Fig. 1(b) are the current density and luminance of the small-area (2×2 mm^2) hybrid tandem white OLED device. The luminous intensity was measured to be 4300 cd/m^2 at the current density of 10 mA/cm^2, whereas the driving voltage was 6.6 V at 1000 cd/m^2. We also measured the luminous efficiency of the device and presented the result in Fig. 1(c). It exhibited the current efficiency of 43.3 cd/A at 10 mA/cm^2. As also shown in the inset in Fig. 1(c), the device showed the Commission Internationale d'Eclairage (CIE) chromaticity coordinates of (0.42, 0.42). Unless otherwise specified hereinafter, the emission area of rectangular-shaped OLED panels is as large as 30×120 mm^2.

Fig. 2 shows the schematic view of opaque and transparent OLED structures with auxiliary metal grids. For an opaque OLED (Fig. 2(a)), an auxiliary metal electrode is deposited and grid patterned on ITO. Those metal lines are then covered with an insulating material. We used Cr, Mo/Al/Mo, or Cu metals as an auxiliary anode. Cr/ITO and Mo/Al/Mo/ITO pre-coated glass substrates were purchased from Geomatech Co., Ltd. The Cu metal was deposited using a sputtering deposition system (SUNICOAT-IS3000, SUNIC SYSTEM) under the DC power of 3000 W (the corresponding deposition rate is 10.2 Å/s). The width of the patterned metals and insulators is 150 and 190 μm, respectively. The distance between the patterned metal lines is ten times greater than the width of each metal line. Namely, the ratio of the emitting area to the non-emitting area is 10:1. For a transparent OLED (Fig. 2(b)), an auxiliary metal electrode can be deposited on a semitransparent cathode in the

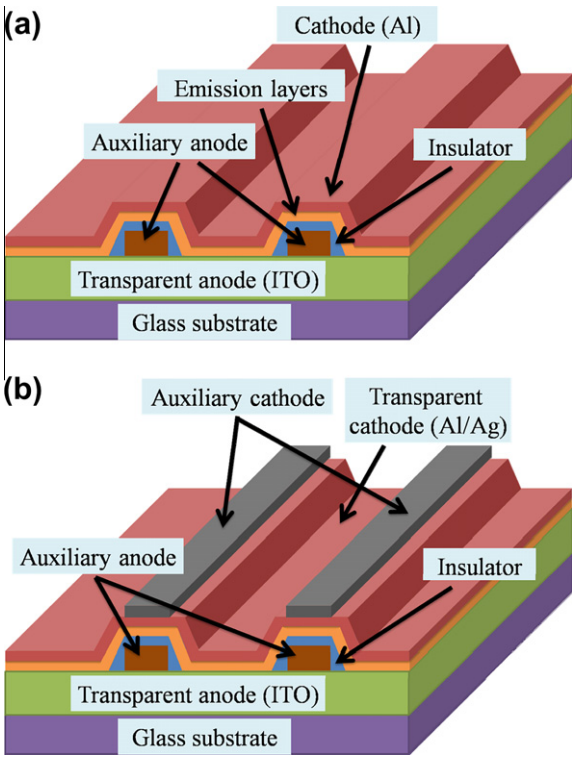

Fig. 2. Schematic view of (a) opaque and (b) transparent OLED structures with auxiliary metal lines.

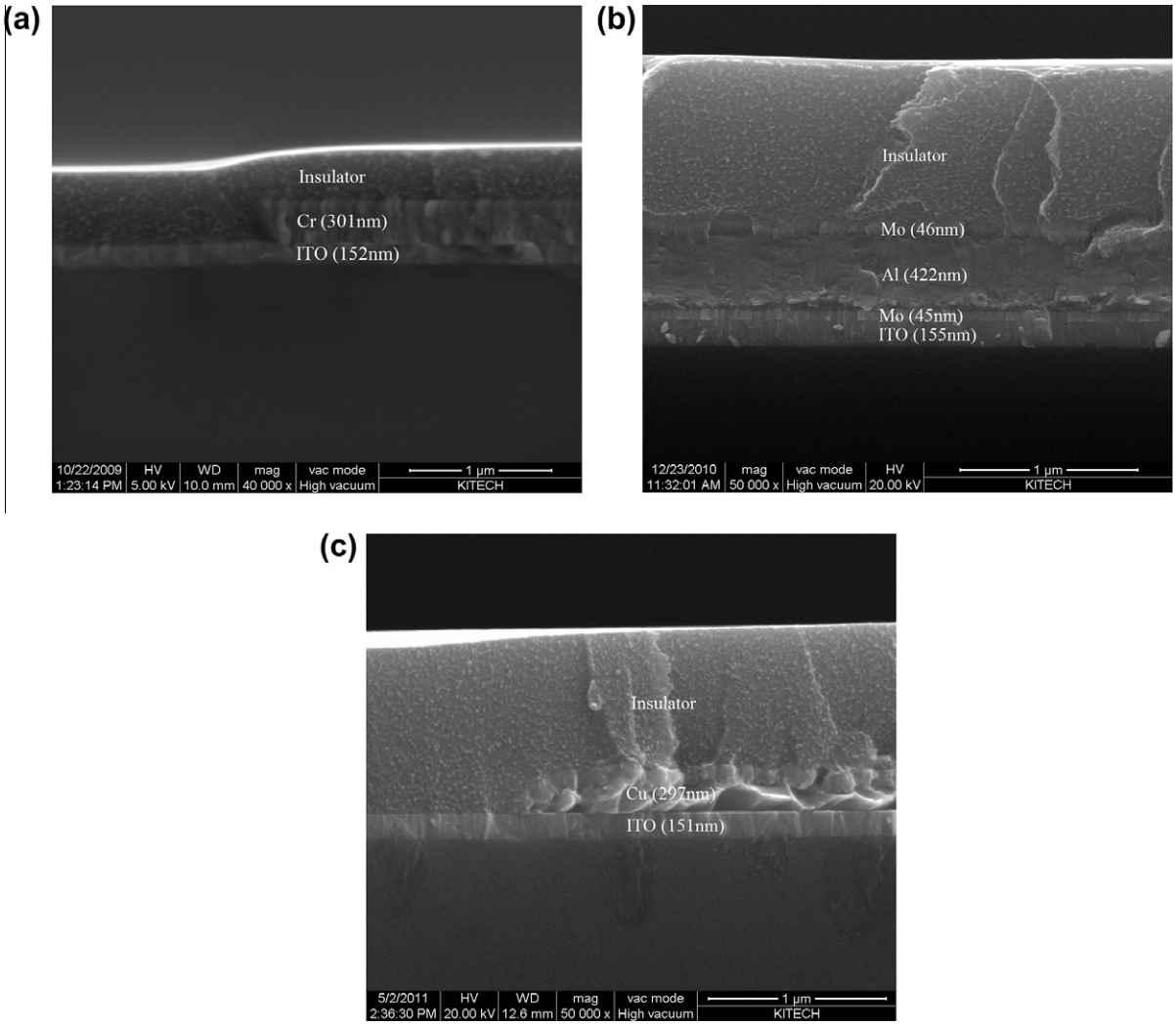

Fig. 3. Scanning electron microscope (SEM) images of a cross-section of (a) Cr, (b) Mo/Al/Mo, and (c) Cu metals on ITO.

presence of the auxiliary anodes. The semitransparent cathode is composed of 1.5-nm-thick Al, 12-nm-thick Ag, and 50-nm-thick NPB. NPB is evaporated to suppress an oxidization of Ag. The sheet resistance of Al/Ag cathode was measured to be as low as 4.5 Ω/□. Such an auxiliary cathode can be deposited using a sputtering system, but it may cause some damage to organic layers. As such, we fabricated it by thermal evaporation of Al (100 nm) using a patterned metal open mask. To maximize the aperture ratio of OLED lighting panels, it is desired to align those auxiliary metal lines for anode and cathode. For simplicity, however, we have chosen the width of Al metal lines to be 2 mm and the distance between them to be 7 mm.

Presented in Fig. 3 are the cross-sectional images of patterned Cr, Mo/Al/Mo, and Cu metal lines measured by field emission scanning electron microscope (FE-SEM, Quanta 200FEG, FEI Co.). The thickness of Cr, Mo, Al, and Cu was measured to be 300, 45, 420, and 297 nm, respectively. The sheet resistance of 300-nm-thick Cr, 513-nm-thick Mo/Al/Mo, and 297-nm-thick Cu on ITO is measured to be 0.7, 0.09, and 0.078 Ω/□, respectively. Although the thickness of Cu metal is lower than that of Mo/Al/Mo metal, its sheet resistance is measured to be even lower. It is attributed that the electrical conductivity ($\sim 5.96 \times 10^7$ S/m [19]) of Cu is higher than that ($\sim 3.5 \times 10^7$ S/m) of Al. Even so, the sheet resistance of Mo/Al/Mo metal is about one order of magnitude lower than that of Cr metal due to the fact that the electrical conductivity of Al is much higher than that ($\sim 7.9 \times 10^6$ S/m) of Cr [20]. As such, the least amount of power loss is expected from OLED with the Cu metal grids, followed by OLED with the Mo/Al/Mo metal grids and then the Cr metal grids.

3. Results and discussion

We have first investigated by way of simulations that an inhomogeneous current distribution becomes more pronounced for large-area TOLED devices when the conductivity of a semitransparent cathode is relatively low. To this

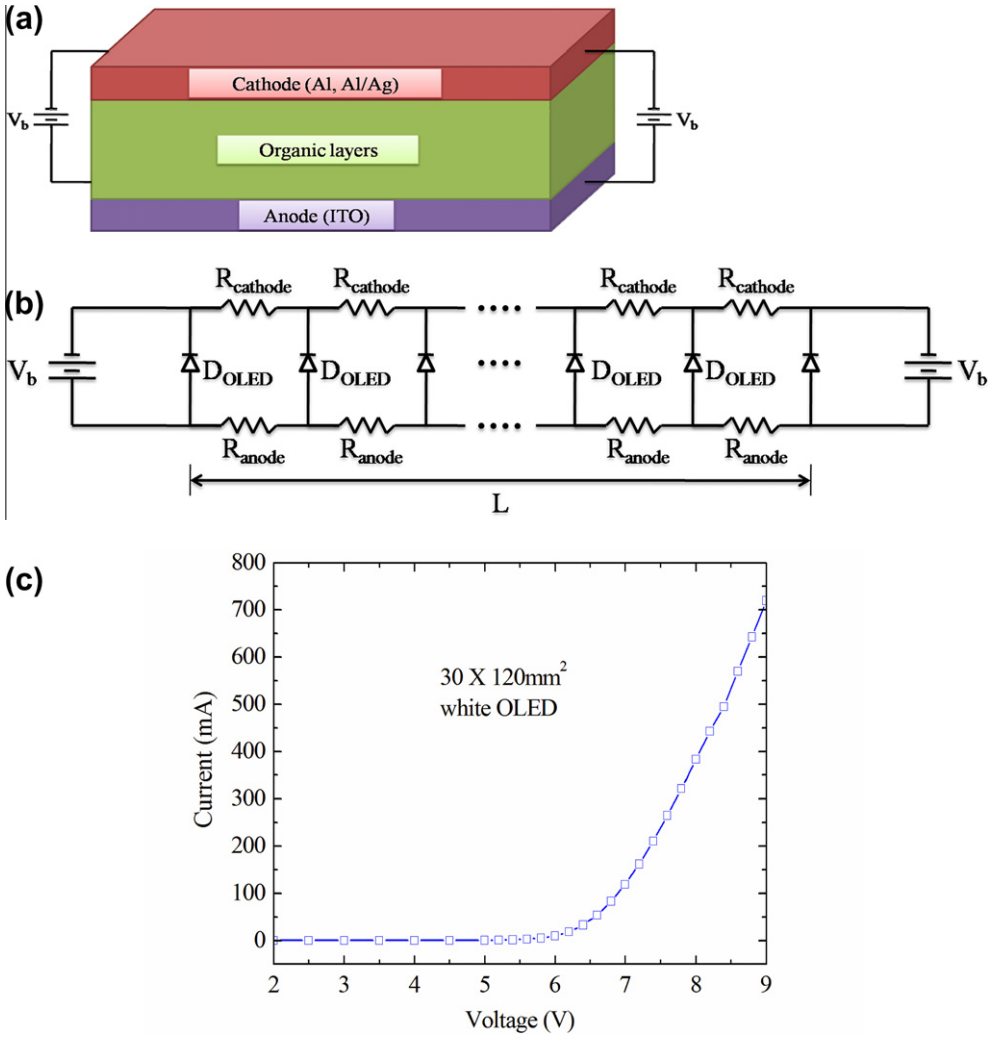

Fig. 4. (a) Schematic view of OLED device structure, (b) its equivalent circuit model, and (c) *IV* curve measured from the hybrid tandem white OLED.

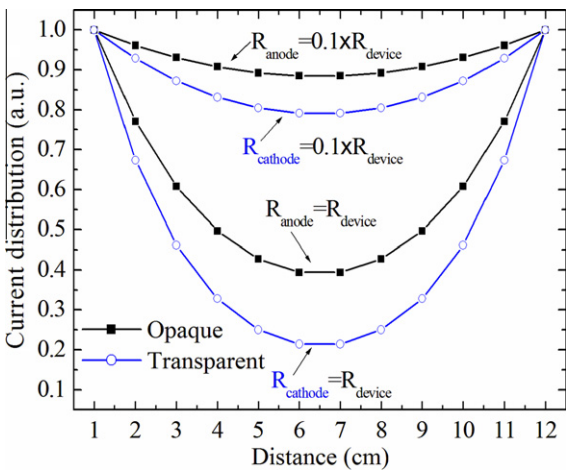

Fig. 5. Simulation results of current distribution of opaque and transparent OLEDs for different horizontal resistances of electrodes.

end, we need to solve a 3-D equivalent circuit model. Though it provides more accurate results, yet it requires a lot of computational efforts. For simplicity, we have simulated the 1-D equivalent circuit model of OLEDs (Fig. 4(a) and (b)) using Cadence OrCAD software [21]. The OLED device is represented by a diode where the *IV* curve (Fig. 4(c)) measured from the hybrid tandem white OLED device is inputted. In Fig. 4(b), R_{anode} indicates the horizontal resistance of anode and $R_{cathode}$ the horizontal resistance of cathode. The vertical device resistance (R_{device}) of OLED is incorporated in the *IV* curve of the diode, which is measured to be about 3.8 Ω. For simulations, we have chosen the total device length (L) to be 120 mm, which is the same as that of the rectangular-shaped OLED panel. We have placed the voltage sources (DC 8.0 V) at both ends of the device. Shown in Fig. 5 is the simulation result of current distribution of opaque and transparent OLEDs for different horizontal resistances of electrodes. When R_{anode} increases from 0.38 Ω (=0.1 × R_{device}) to 3.8 Ω (=R_{device}) for opaque OLEDs, the current uniformity is degraded from 88% to 40%.

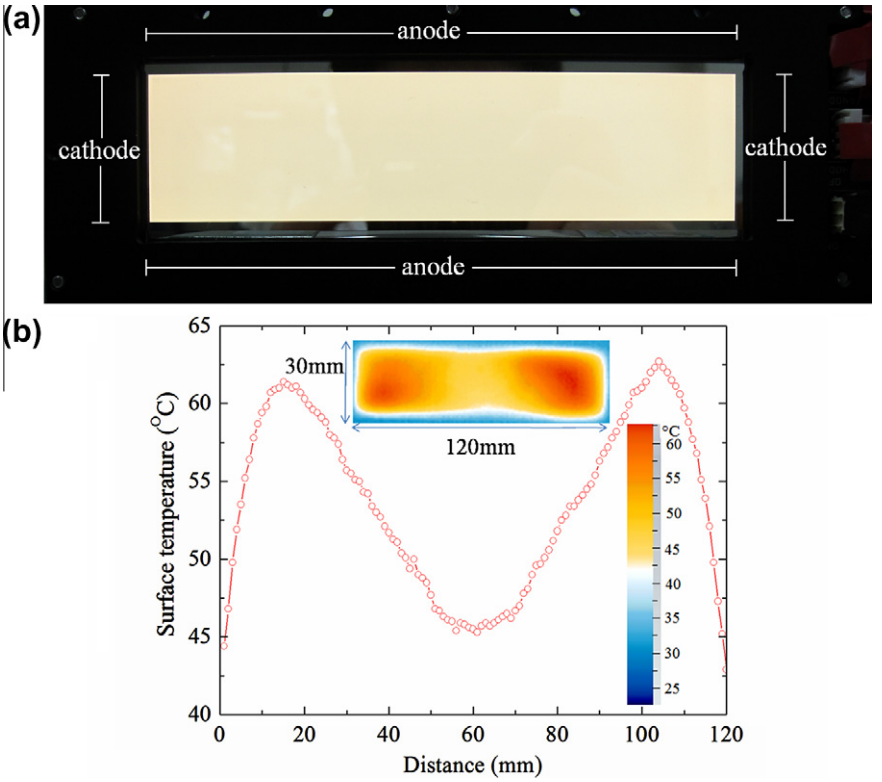

Fig. 6. (a) Image of light emission (at 1000 nit) and (b) surface temperature distribution (at 5000 nit) of hybrid tandem white OLED without any auxiliary electrode included (ITO only). Inset in (b) is the thermal image of the OLED panel (30×120 mm^2) and scale bar.

Namely, more current flows through OLED near the panel edges rather than its central region at higher R_{anode}. It is also seen that a voltage drop is more pronounced in TOLEDs. When $R_{cathode} = 0.38\ \Omega$ (=$0.1 \times R_{device}$), the current uniformity (80%) of TOLED is lower than that (88%) of opaque OLED with the same R_{anode}. It is further decreased from 40% to 20% when $R_{cathode} = 3.8\ \Omega$ (=R_{device}). The non-uniform current distribution induced by the low electrical conductivity of electrodes causes the non-uniform luminance distribution because the luminous intensity is proportional to the current density (see Fig. 1(b)). We demonstrated in [6] that the ratio between R_{anode} and R_{device} of opaque OLED devices is the critical factor to determine the luminance uniformity. In addition, the simulation results imply that we also need to consider the ratio between $R_{cathode}$ and R_{device} in designing large-area TOLED lighting panels because of the limiting conductivity of a transparent cathode. Therefore, not only an anode but also a cathode may require metallic grids for large-area TOLED lighting panels.

As a reference device, we fabricated 30×120 mm^2 hybrid tandem white OLED panels without any metallic grids included. To ensure uniform current injection, we used multi-pin contacts at the interface between the electrodes and a driving circuit. Those pins are connected each other through copper wires. This scheme removes external factors that may affect the emission uniformity and heat generation. Fig. 6 shows the image of light emission and surface temperature distribution of the white OLED panel. As evident in Fig. 6(b), a highly non-uniform surface temperature distribution is observed from the white OLED panel in the absence of auxiliary metal electrodes. The maximum temperature difference between edge and center areas was over 17.4 °C at 5000 nit. Such local heat generation appears because a large amount of current is concentrated at both ends of the rectangular-shaped panel (i.e., near the electrodes). This would degrade the overall device performance (i.e., power efficacy and luminance uniformity) and stability. In fact, the Joule heating problem is always parasitic on the devices. The Joule heating in the organic stack induced by high current injection during operation can be written as [22]

$$H_{Org} = \left[\frac{J_n(x,t)^2}{q\mu_n(x,t)n(x,t)} + \frac{J_p(x,t)^2}{q\mu_p(x,t)p(x,t)}\right] \tag{3}$$

with the variables J defined as the current density, μ_n the electron mobility, μ_p the hole mobility, n the electron density, and p the hole density. Meanwhile, the heat generation by electric conductors (i.e., anode and cathode) carrying current (I) is given as

$$H_{Anode,Cathode} = I^2R. \tag{4}$$

It is proportional to the electrical resistance (R) of the conductor. The total Joule heating is the sum of electrical losses in the three conducting layers (i.e., $H_{Total} = H_{Anode} + H_{Org} + H_{Cathode}$) [23]. Therefore, the electrodes with high electrical conductivity are highly demanded to suppress local heat generation.

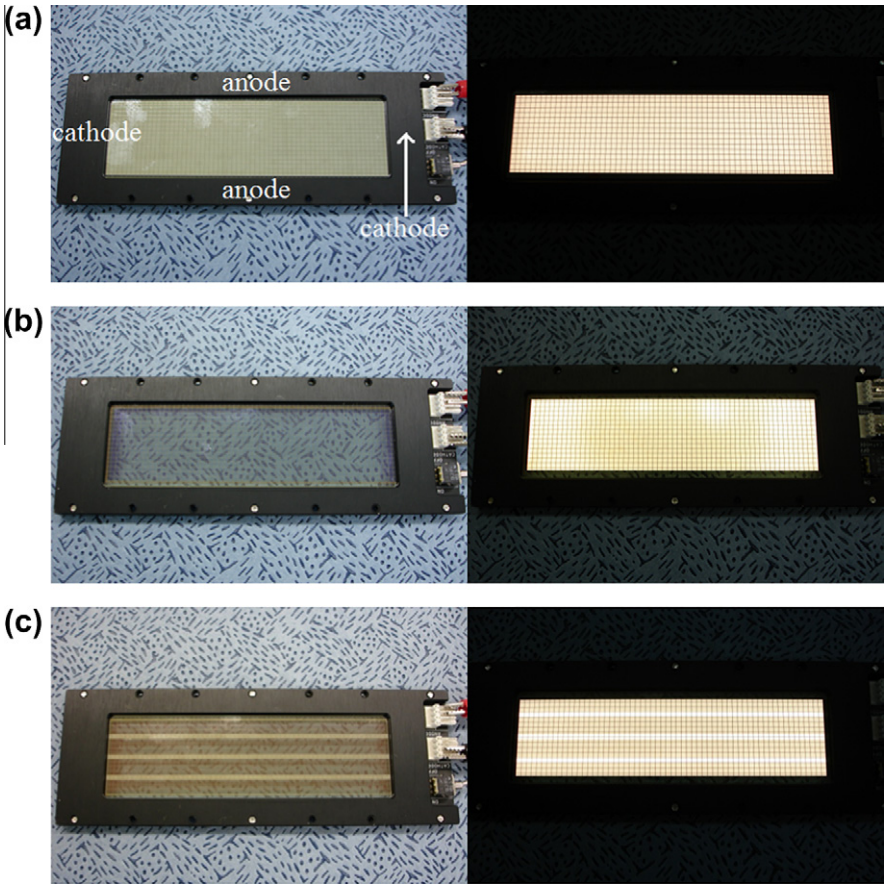

Fig. 7. Images of light emission from (a) opaque and (b) transparent OLED lighting panels with the auxiliary Cr metal lines on ITO and (c) transparent OLED panel with both auxiliary Cr on ITO and Al metal lines on the transparent cathode.

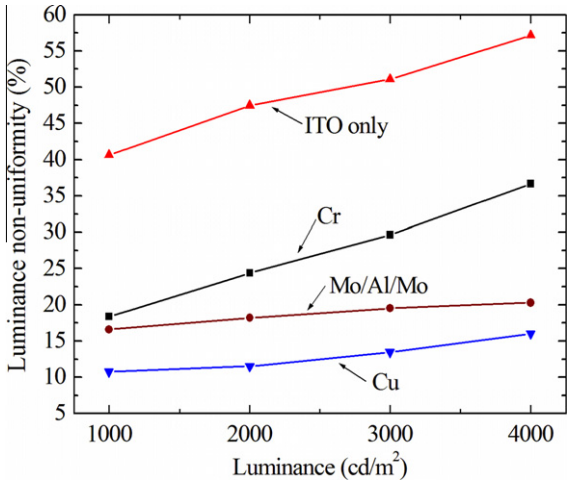

Fig. 8. Luminance non-uniformity versus luminous intensity measured from $30 \times 120\ mm^2$ opaque OLEDs for different auxiliary metal grids.

With attempt to enhance the overall device performance, we have fabricated 30 mm × 120 mm white OLED panels with those auxiliary electrodes included. Fig. 7(a) shows the image of light emission from the opaque OLED lighting panel with the Cr metal grids on the ITO anode. Presented in Fig. 7(b) is the image of light emission from the TOLED panel with the Cr metal grids on ITO in the absence of the auxiliary Al metal lines on the Al/Ag cathode, and in Fig. 7(c) the TOLED panel with both auxiliary metal grids on anode and cathode. In the presence of the auxiliary Al metal lines on the Al/Ag cathode, higher luminous intensity is observed along the Al metal lines in the case of bottom emission (i.e., emission through ITO), which originates from the reflection of light by them. Though this feature may degrade the luminance uniformity, yet it

Table 1
Luminance non-uniformity of $30 \times 120\ mm^2$ opaque OLED panels for different average luminances.

	1000 nit (%)	2000 nit (%)	3000 nit (%)	4000 nit (%)
ITO only	40.65	47.46	51.09	57.16
Cr	18.38	24.37	29.64	36.68
Mo/Al/Mo	16.6	18.2	19.51	20.28
Cu	10.76	11.52	13.46	16.02

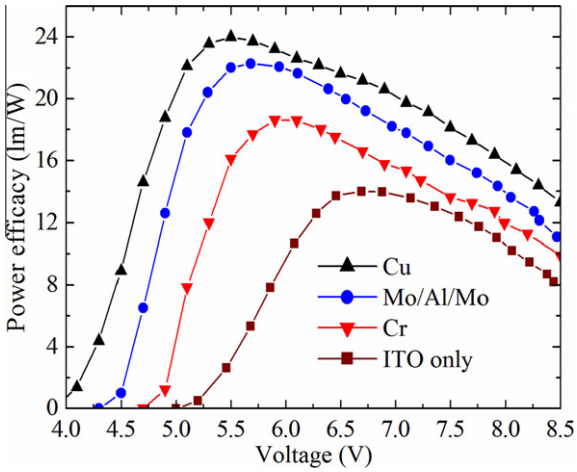

Fig. 9. Power efficacy versus applied bias voltage of $30 \times 120\ mm^2$ opaque OLEDs for different auxiliary metal grids.

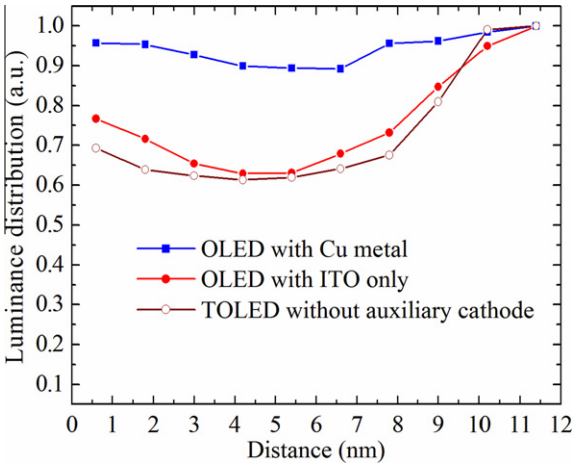

Fig. 11. Luminance distribution of OLED panels measured at the average luminance of 1000 nit.

suppresses local heat generation to a great extent, which will be addressed later with experiment results. We have measured the luminance non-uniformity of those panels using 2D color analyzer (CA-2000A, Konica Minolta). Fig. 8 shows the luminance non-uniformity of opaque OLEDs with respect to luminous intensity for different metallic grids. We measured the luminance at 50 spots selected over the emission area ($30 \times 120\ mm^2$) and quantified the luminance non-uniformity at different average luminances. The measured results are also summarized in Table 1. The luminance uniformity decreased with increasing luminous intensity in all devices. As expected, the OLED device with the Cu metal grids exhibits the lowest luminance non-uniformity. Moreover, the OLED devices with high conductivity Cu or Mo/Al/Mo metal grids showed a few percent increases (<6%) of luminance non-uniformity with increasing luminous intensity from 1000 nit to 4000 nit. One the other hand, it is observed that the OLED devices with bare ITO or the Cr metal grids showed a steeper rise in the luminance non-uniformity (>15%) with increasing luminous intensity due to its lower electrical conductivity.

We have measured the power efficacy of those opaque OLED panels using an integrating sphere (Neolight PL5000, PIMACS Co. Ltd.) and presented the results in Fig. 9. The OLED panel with the Cu metal grids shows the highest power efficacy (24 lm/W at 5.5 V), followed by the OLED panel (22.27 lm/W at 5.68 V) with the Mo/Al/Mo metal grids and then the OLED panel (18.63 lm/W at 5.9 V) with the Cr metal grids. The OLED panel without any metal grids (with ITO only) exhibits the lowest power efficacy (14 lm/W at 6.69 V) owing to a high power loss. It is observed that high-conductivity metallic grids lower the driving voltage and consequently enhance the power efficacy. Such a positive effect is also observed in local heat generation or surface temperature distribution. As evident in Fig. 10, heat generation is much suppressed by the Cu metal grids. At the luminous intensity of 3000 nit, the maximum temperature (46.5 °C) of OLED with the Cr metal grids is reduced to 44.4 °C with the Mo/Al/Mo and further reduced to 42.2 °C with the Cu metal grids.

As discussed earlier with simulation results, non-uniform light emission and heat generation may be more pronounced when both electrodes (anode and cathode) show relatively high resistance. Since the sheet resistance (4.5 Ω/□) of the Al/Ag cathode is still too high, such phenomena may appear in large-area TOLED panels even in the presence of metallic grids on ITO. As apparent in

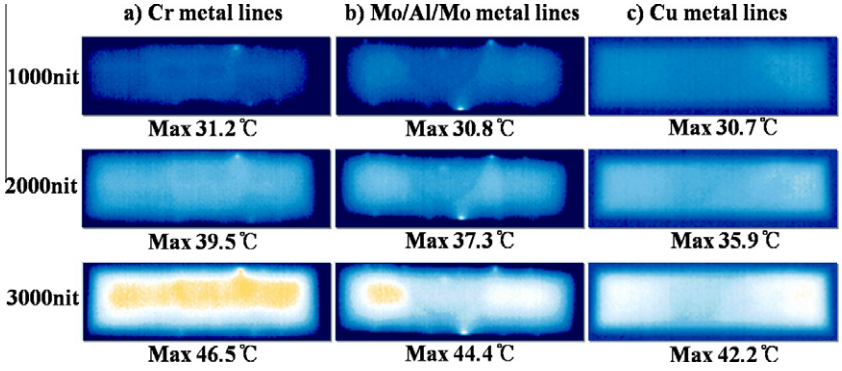

Fig. 10. Comparison in heat distribution of $30 \times 120\ mm^2$ opaque OLEDs for different auxiliary metal grids measured at different average luminances.

Table 2
Luminance non-uniformity of 30 × 120 mm^2 TOLED panels with the Cr metal grids on ITO according to the existence of the Al metal lines on the transparent cathode for different average luminances.

		1000 nit (%)	2000 nit (%)	3000 nit (%)	4000 nit (%)
Without auxiliary cathode	Bottom (ITO side)	44.61	49.38	54.34	70
	Top (cathode side)	44.34	54.48	61.4	71.44
With auxiliary cathode	Bottom (ITO side)	50.65	51.49	52.89	53.13
	Top (cathode side)	–	–	–	–

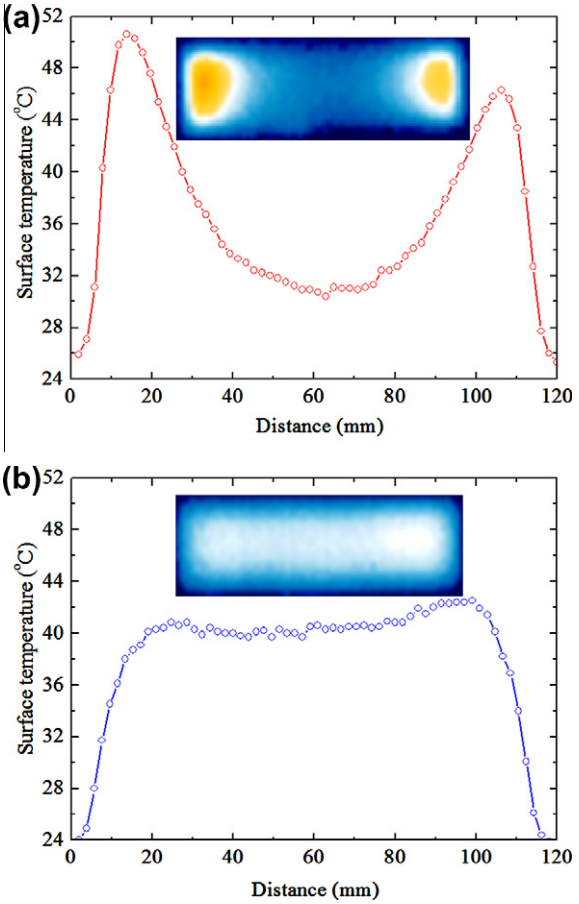

Fig. 12. Measured surface temperature distribution of transparent OLEDs (a) without and (b) with the auxiliary Al metal lines at the average luminance of 2000 nit. Insets are thermal images.

Fig. 11, the luminance distribution of opaque OLED with ITO only is very similar to that of TOLED with the Cr metal grids on ITO but without an auxiliary electrode on the transparent cathode. This result indicates that an auxiliary metal is required not only on the ITO anode but also on the Al/Ag cathode for large-area TOLEDs to reduce such a power loss in Fig. 9. We measured the luminance non-uniformity of 30 × 120 mm^2 TOLED panels with the Cr metal lines on ITO and the Al metal lines on the transparent Al/Ag cathode for different average luminances and summarized the results in Table 2. Since the TOLED device emits light from both sides of the panel, we measured the average luminances at each side and added them together. Due to a relatively low transparency of the Al/Ag cathode (~60% at 550 nm), higher luminance was measured from the bottom side of the panel, i.e., more light emits through the ITO anode. Because a line-shaped high luminance contrast was observed from the bottom side (ITO side) of the TOLED panel due to the reflection of light by the auxiliary Al metal lines (Fig. 7(c)), its luminance non-uniformity (50.65% at 1000 nit) is a little higher at low luminous intensities, compared with the TOLED without the auxiliary Al metal lines (44.61%). At higher luminous intensities, however, a steep increase of the luminance non-uniformity appeared at the device without the auxiliary Al metal lines on the semitransparent metal cathode. Such a phenomenon disappeared in the presence of the Al metal lines, a feature highly desirable for transparent lighting applications.

Although the Al metal lines on the transparent cathode degrade the luminance uniformity, they play an important role in suppressing local heat generation. As shown in Fig. 12(a), a highly non-uniform heat distribution is observed and local heat generation is pronounced without the Al metal lines. In other words, a steep temperature rise occurs at both ends of the panel. It is attributed that a current density is concentrated near the panel edges instead of reaching its central region due to a relatively high R_{anode} and $R_{cathode}$, compared with R_{device}. However, it can be effectively suppressed by the insertion of auxiliary Al metal lines, as evident in Fig. 12(b). Even though the average temperature (37.3 °C) of TOLED without auxiliary Al lines is slightly lower than that (39.6 °C) of TOLED with them, yet its temperature uniformity is much degraded without Al metal lines, possibly causing a reduction of device lifetime and reliability. As such, an auxiliary metallic grid on a transparent cathode is also essential for large-area TOLED lighting panels.

As aforementioned, the shape of the light-emitting area can affect the luminance and heat distributions. To verify it, we fabricated three different shapes of large-area OLED panels; rectangular- (30 × 120 mm^2), square- (70 × 70 mm^2), and round-shaped (diameter = 70 mm) with the Mo/Al/Mo metal grids. The rectangular- and square-shaped panels consist of the same square-shaped grids (150 μm in width), while the round-shaped one has the hexagonal grids (h = 1 mm) (see Fig. 13). The luminance non-uniformity measured from those panels for different average luminances was summarized in Table 3. The round-shaped OLED panel exhibits the highest luminance uniformity at all measured average luminances (1000–4000 nit), followed by the square-shaped and then the rectangular-shaped panel. Fig. 13(a) and (b) shows the images of white light emission from square- and round-shaped panels and measured surface temperature distributions at 8 V, respectively. It is also recognizable even with the naked eye that the round-shaped panel exhibits a highly homogeneous

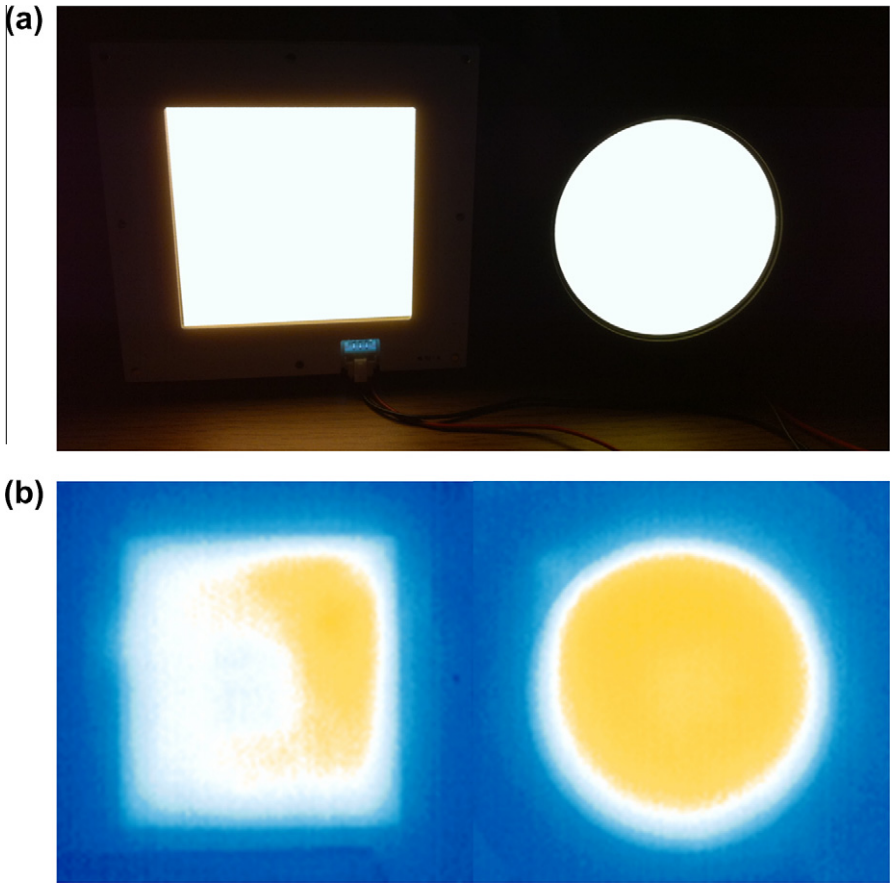

Fig. 13. (a) Images of white light emission from square- and round-shaped OLED panels and (b) their surface temperature distributions measured under the bias voltage of 8 V.

Table 3
Luminance non-uniformity of opaque OLEDs in different shape with the Mo/Al/Mo metal grids on ITO for different average luminances.

	1000 nit (%)	2000 nit (%)	3000 nit (%)	4000 nit (%)
Rectangle (30×120 mm^2)	16.6	18.2	19.51	20.28
Square (70×70 mm^2)	6.17	11.1	14.68	27.67
Round (diam = 70 mm)	5.22	6.85	12.22	14.7

heat distribution. For square- and rectangular-shaped OLEDs, the hottest spots always appear near the corners or both ends of the panels where holes injected from each side of the auxiliary anode surrounding the light-emitting area are merged. In this context, the number of sides for the shape of the light-emitting area or the metallic grid is desired to be high [16]. Namely, the round-shaped panel is favored the most as the number of sides is infinite, followed by the hexagonal-shaped panel (the number of sides is 6), the square-shaped panel (the number of sides is 4), and then the triangular-shaped panel (the number of sides is 3).

4. Conclusion

We investigated the effects of auxiliary metal electrodes on the optical and thermal properties of large-area white OLED and TOLED lighting panels. Non-uniform light emission and local heat generation in opaque OLEDs were effectively suppressed with grid-patterned auxiliary Cu electrodes due to its high conductivity. In addition, local heat generation was effectively reduced in TOLED panels by the insertion of both auxiliary Cr metal grids on an ITO anode and auxiliary Al metal lines on a semitransparent cathode, though TOLEDs showed a decrease of luminance uniformity due to wide Al metal lines. Finally, we studied the effect of the shape of light-emitting areas and metal grid patterns on the luminance uniformity and heat distribution of white OLED devices. The round-shaped panel with hexagonal grids showed the most homogeneous heat and luminance distributions.

Acknowledgment

This work was supported by the IT R&D Program of MKE/IITA. [2009-F-016-01, Development of Eco-Emotional OLED Flat-Panel Lighting].

References

[1] K. Leo, Science 310 (2005) 1762.
[2] Y. Sun, N. Giebink, H. Kanno, B. Wa, M.E. Thompson, S.R. Forrest, Nature (London) 440 (2006) 908.
[3] B. D'Andrade, J. Esler, C. Lin, M. Weaver, J. Brown, SID08 Digest (2008) 940.
[4] J. Kido, High performance OLEDs for displays and general lighting, SID08 (2008) 931.
[5] Joerg Amelung, Large-area Organic Light-emitting Diode Technology, <http://spie.org/x23960.xml>.
[6] J.W. Park, J.H. Lee, D.C. Shin, S.H. Park, IEEE/OSA J. Display Technol. 5 (2009) 306.
[7] L. Pohl, E. Kollár, Zs. Kohári, A. Poppe, Therminic (2008) 235.
[8] C. Gärditz, A. Winnacker, F. Schindler, R. Paetzold, Appl. Phys. Lett. 90 (2007) 103506.
[9] J. Kido, Proc. SPIE 7051 (2008) 705169.
[10] K. Neyts, M. Marescaux, A.U. Nieto, A. Elschner, W. Lövenich, K. Fehse, Q. Huang, K. Walzer, K. Leo, J. Appl. Phys. 100 (2006) 114513.
[11] S.Y. Ryu, J.H. Noh, B.H. Hwang, C.S. Kim, S.J. Jo, J.T. Kim, H.S. Hwang, H.K. Baik, H.S. Jeong, C.H. Lee, S.Y. Song, S.H. Choi, S.Y. Park, Appl. Phys. Lett. 92 (2008) 023306.
[12] K.S. Yook, S.O. Jeon, C.W. Joo, J.Y. Lee, Appl. Phys. Lett. 93 (2008) 013301.
[13] D.R. Sahu, S.-Y. Lin, J.-L. Huang, Thin Solid Films 516 (2008) 4728.
[14] L. Cattin, M. Morsli, F. Dahou, S. Yapi Abe, A. Khelil, J.C. Bernède, Thin Solid Films 518 (2010) 4560.
[15] K. Hong, K. Kim, S. Kim, I. Lee, H. Cho, S. Yoo, H.W. Choi, N.-Y. Lee, Y.-H. Tak, J.-L. Lee, J. Phys. Chem. C 115 (2011) 3453.
[16] K. Neyts, A. Real, M. Marescaux, S. Mladenovski, J. Beeckman, J. Appl. Phys. 103 (2008) 093113.
[17] D. Selvanathan, F.M. Mohammed, A. Tesfayesus, I. Adesida, J. Vac. Sci. Technol. B 22 (2004) 2409.
[18] D.H. Kim, N.S. Cho, H.-Y. Oh, J.H. Yang, W.S. Jeon, J.S. Park, M.C. Suh, J.H. Kwon, Adv. Mater. 23 (2011) 1.
[19] http://en.wikipedia.org/wiki/Electrical_resistivity_and_conductivity.
[20] http://www.chemicool.com/elements/chromium.html#conductivity.
[21] http://www.cadence.com/products/orcad/Pages/default.aspx.
[22] J.W. Park, H.K. Ham, C.Y. Park, Org. Electron. 12 (2011) 227–233.
[23] M. Slawinski, D. Bertram, M. Heuken, H. Kalisch, A. Vescan, Org. Electron. 12 (2011) 1399.